Tune-out and magic wavelengths of Ba^+ ions

Jun Jiang,* Yun Ma, Xia Wang, Chen-Zhong Dong, and Z. W. Wu

Key Laboratory of Atomic and Molecular Physics and Functional Materials of Gansu Province, College of Physics and Electronic Engineering, Northwest Normal University, Lanzhou 730070, People's Republic of China

(Received 29 October 2020; accepted 8 February 2021; published 3 March 2021)

The static and dynamic polarizabilities of the ground state and low-lying excited states of Ba^+ ions are calculated by using a relativistic semiempirical method: the relativistic configuration interaction plus core polarization (RCICP) method. The tune-out wavelengths of the ground state and magic wavelengths of the $6s_{1/2} \rightarrow 6p_{1/2,3/2}, 5d_{3/2,5/2}$ transitions are determined. One visible tune-out wavelength, 480.658(18) nm, is found. High-precision measurements on this tune-out wavelength could be used to determine the ratio of the oscillator strengths of the $6s_{1/2} \rightarrow 6p_{1/2,3/2}$ transitions. In addition, we suggest that the measurements on the magic wavelengths corresponding to the $6s_{1/2} \rightarrow 5d_{3/2,5/2}$ transitions could be used to determine the oscillator strengths of the $5d_{5/2} \rightarrow 4f_{7/2}$ and $5d_{3/2} \rightarrow 4f_{5/2}$ transitions, while the measurements of the magic wavelengths near 416 nm for the $6s_{1/2} \rightarrow 6p_{3/2}$ transition could be used to determine the ratio of the oscillator strengths of the $6p_{3/2} \rightarrow 6d_{3/2,5/2}$ transitions.

DOI: 10.1103/PhysRevA.103.032803

I. INTRODUCTION

The technique of manipulating atoms by using lasers has been widely used in high-precision measurements, such as atomic clocks [1–6], atomic magnetometers [7–10], and atomic interferometers [8,11–13]. However, the interaction between laser fields and atoms can cause ac Stark shift which would affect the accuracy of the measurement for relevant atomic parameters. In order to reduce the impact of the ac Stark shift, magic-wavelength trapping was introduced in Refs. [14,15], in which the shifts of a given pair of energy levels are the same as each other. Based on the magic-wavelength trapping, the uncertainties of high-precision measurements of atomic parameters are reduced remarkably [16,17]. Moreover, a quantity called tune-out wavelength, at which the dynamic dipole polarizability for a given state is equal to zero, was also introduced by LeBlanc and Thywissen [18]. Since the polarizability is zero, the dipole interactions between atoms and the laser fields vanish as well. Atoms trapped in an optical lattice can be released by tuning the wavelength of trapping laser to be the tune-out wavelength of those atoms. Therefore, tune-out wavelengths can be used in the sympathetic cooling of atoms [5,18–22]. Furthermore, the technique of all-optical trapping of atoms and ions also provides a practical method to measure the tune-out wavelength very accurately, which is effectively a null experiment since it measures the frequency when the polarizability is zero and does not rely on a precise determination of the intensity of a laser field.

In particular, the accurate determination of tune-out and magic wavelengths of atoms and ions plays an important role in testing atomic structure calculations and providing some important parameters. For example, the tune-out wavelengths for Rb [19,23–25], K [26,27], Li [28], Dy [29], and He [30,31] atoms have been measured with very high accuracy, and thereby the ratios of the corresponding line strengths of the transitions involved have also been determined very accurately following the method described later in this paper.

Ba^+ is one of the very good candidates for ionic clock experiments [32,33], quantum information techniques [34–36], and atomic parity-violation experiments [37]. Detailed information of Ba^+ ions, such as the electric-dipole ($E1$) matrix elements, polarizabilities, tune-out wavelengths, and magic wavelengths, is thus of great importance to these experiments. Recently, a magic wavelength for the clock transition $6s_{1/2} \rightarrow 5d_{5/2}$ of $^{138}Ba^+$ ions was measured with an uncertainty of a few GHz [38]. This measurement was used to make an accurate assessment of the room-temperature blackbody radiation (BBR) shift. In addition, a far-off-resonance optical trap of the Ba^+ ion has been implemented experimentally [39]. This technique makes it possible to measure the tune-out wavelengths of Ba^+ ions with high precision.

In this paper, the energy levels and $E1$ matrix elements as well as the static and dynamic dipole polarizabilities of Ba^+ ions are calculated using a relativistic semiempirical method: the relativistic configuration interaction plus core polarization (RCICP) method. The tune-out wavelengths of the $6s_{1/2}$ state and the magic wavelengths for the $6s_{1/2} \rightarrow 6p_{1/2,3/2}$ and $6s_{1/2} \rightarrow 5d_{3/2,5/2}$ transitions are further determined. The obtained tune-out wavelengths and magic wavelengths are discussed in detail, and can be used to determine other high-precision atomic parameters. Atomic units ($m_e = 1$, $e = 1$, $\hbar = 1$) are used throughout the paper unless stated otherwise. The speed of light is additionally taken to be 137.035 999 1 in our calculations.

II. THEORETICAL METHOD

As a detailed description of the RCICP method has been given in Ref. [40]; here we just present a brief introduction.

*phyjiang@yeah.net

TABLE I. The cutoff parameters $\rho_{\ell,j}$ of the polarization potential of Ba^+ ions.

States	j	$\rho_{\ell,j}$ (a.u.)
s	1/2	2.35337
p	1/2	2.24830
	3/2	2.27064
d	3/2	2.75119
	5/2	2.78043

The key strategy of the method is to partition a Ba^+ ion into a Ba^{2+} core plus a valence electron. The first step involves a Dirac-Fock (DF) calculation on the core of Ba^+ ions. The single-particle orbitals are written as a linear combination of the S-spinors [41–45] which can be regarded as a relativistic generalization of the Slater-type orbitals.

The effective Hamiltonian of the valence electron is written as

$$H = c\boldsymbol{\alpha}\cdot\boldsymbol{p} + (\beta - 1)c^2 + V_{\rm core}(\boldsymbol{r}), \tag{1}$$

where $\boldsymbol{\alpha}$ and β denote the 4×4 Dirac matrices, $\boldsymbol{p}$ is the momentum operator, c is the speed of light, and $\boldsymbol{r}$ is the position vector of the valence electron. Moreover, $V_{\rm core}(\boldsymbol{r})$ is given by

$$V_{\rm core}(\boldsymbol{r}) = -\frac{Z}{r} + V_{\rm dir}(\boldsymbol{r}) + V_{\rm exc}(\boldsymbol{r}) + V_{\rm p}(\boldsymbol{r}). \tag{2}$$

Here, Z is atomic number, r is the distance of the valence electron with respect to the origin of the coordinates. $V_{\rm dir}(\boldsymbol{r})$ and $V_{\rm exc}(\boldsymbol{r})$ denote the direct and exchange interactions of the valence electron with the core electrons, respectively. The ℓ- and j-dependent polarization potential $V_{\rm p}(\boldsymbol{r})$ can be written as

$$V_{\rm p}(\boldsymbol{r}) = -\sum_{k=1}^{2}\frac{\alpha^k_{\rm core}}{2r^{2(k+1)}}\sum_{\ell,j} g^2_{\ell,j}(r)|\ell j\rangle\langle\ell j|, \tag{3}$$

where ℓ and j are the orbital and total angular momenta, respectively. $\alpha^k_{\rm core}$ is the kth-order static polarizabilities of the core electrons ($\alpha^1_{\rm core} = 10.61$ a.u. and $\alpha^2_{\rm core} = 46.0$ a.u. for Ba^{2+} ions [46]), and $g^2_{k,\ell,j}(r) = 1 - \exp(-r^{2(k+2)}/\rho^{2(k+2)}_{\ell,j})$. The cutoff parameters $\rho_{\ell,j}$ are tuned to reproduce the binding energies of the ground state and some low-lying excited states, and the adopted parameters are listed in Table I. The effective Hamiltonian of the valence electron is diagonalized within a large S-spinor and L-spinor basis [44,47]. L-spinors can be regarded as a relativistic generalization of the Laguerre-type orbitals.

The energy levels of some low-lying states of Ba^+ ions are listed in Table II, comparing with available experimental energies from the National Institute of Science and Technology (NIST) tabulation [48]. It can be found that the present RCICP results are in good agreement with those from the NIST tabulation.

TABLE II. Energy levels (cm^{-1}) of some low-lying states of Ba^+ ions. The relevant energies are given relatively to the energy of the core Ba^{2+}. The experimental data are taken from the National Institute of Science and Technology (NIST) tabulation [48].

States	J	RCICP	Expt.
$6s$	1/2	−80686.30	−80686.30
$5d$	3/2	−75812.45	−75812.45
	5/2	−75011.49	−75011.49
$6p$	1/2	−60424.74	−60424.74
	3/2	−58733.91	−58733.90
$7s$	1/2	−38273.33	−38331.13
$6d$	3/2	−34419.10	−34736.83
	5/2	−34209.99	−34531.45
$4f$	5/2	−32427.67	−32427.68
	7/2	−32202.99	−32202.97
$7p$	1/2	−31250.17	−31296.48
	3/2	−30628.92	−30674.96
$8s$	1/2	−22625.21	−22661.09
$5f$	5/2	−22623.81	−23295.38
	7/2	−22387.30	−23054.56
$7d$	3/2	−20709.15	−20886.05
	5/2	−20611.83	−20791.37
$8p$	1/2	−19336.49	−19346.77
	3/2	−19011.94	−19044.33

III. RESULTS AND DISCUSSION

A. Dipole transition matrix elements

The $E1$ transition matrix elements are calculated with a modified dipole transition operator given by [49–53]

$$\boldsymbol{D} = \boldsymbol{r} - \left[1 - \exp\left(-\frac{r^6}{\rho^6}\right)\right]^{1/2}\frac{\alpha^1_{\rm core}\boldsymbol{r}}{r^3}. \tag{4}$$

The cutoff parameter ρ is 2.4596 a.u., generated as $\rho = \frac{1}{6}(2\rho_{s_{1/2}} + \rho_{p_{1/2}} + \rho_{p_{3/2}} + \rho_{d_{3/2}} + \rho_{d_{5/2}})$.

Table III lists the presently calculated $E1$ reduced matrix elements for some important transitions, along with a comparison with some available theoretical [54–59] and experimental results [60–65]. The uncertainties of the matrix elements given in the table are estimated using the method in our previous calculations for Cs atoms [66]. For the resonant $6s_{1/2} \to 6p_{1/2,3/2}$ transitions, which are dominant contributing to the polarizability of the ground state, the present RCICP results are found to be smaller than the experimental [61] and theoretical results [54–59] by only about 1.5%. For the $5d_{3/2,5/2} \to 6p_{1/2,3/2}$, $5d_{3/2,5/2} \to 4f_{5/2,7/2}$, $6p_{1/2,3/2} \to 7s_{1/2}$, and $6p_{1/2,3/2} \to 6d_{3/2,5/2}$ transitions, the reduced matrix elements are all larger than 1.0 a.u., and the present RCICP results agree very well with the experimental and other theoretical results. The agreement with the measurements is better than 2%. Moreover, for the $6s_{1/2} \to 7p_{1/2,3/2}$, $6s_{1/2} \to 8p_{1/2,3/2}$, $5d_{3/2,5/2} \to 7p_{1/2,3/2}$, and $5d_{3/2,5/2} \to 8p_{1/2,3/2}$ transitions, the reduced matrix elements are all less than 1.0 a.u. and no experimental results can be found. Nevertheless, the present results show a good agreement with the calculations from the relativistic many-body perturbation theory all-order method (RMBPT all-order) [58],

TABLE III. Reduced E1 matrix elements (a.u.) for principal transitions of Ba^+ ions. The numbers in the parentheses are uncertainties.

Transitions	RCICP	RMBPT RCC[a] [54]	RMBPT all-order[b] [58]	SD RCCSDT[c] [55]	SD all-order[d] [59]	LCC[e] [56]	SDpT[f] [57]	Expt.
$6s_{1/2} \to 6p_{1/2}$	3.275(47)	3.36(1)	3.310	3.3266	3.3357		3.3710	3.36(4) [60], 3.3251(21) [61], 3.327(7) [62]
$6s_{1/2} \to 6p_{3/2}$	4.637(67)	4.73(3)	4.674	4.6982	4.7065		4.7569	4.55(10) [60], 4.7017(27) [61], 4.705(11) [62], 4.720(40) [63]
$6s_{1/2} \to 7p_{1/2}$	0.10(5)	0.10(1)	0.099	0.1193	0.0621	0.061	0.0607	
$6s_{1/2} \to 7p_{3/2}$	0.04(2)	0.17(5)	0.035	0.3610	0.0868	0.087	0.0858	
$6s_{1/2} \to 8p_{1/2}$	0.11(6)	0.11(5)	0.115	0.4696		0.087	0.0866	
$6s_{1/2} \to 8p_{3/2}$	0.06(3)	0.11(5)	0.073	0.5710		0.033	0.0334	
$5d_{3/2} \to 6p_{1/2}$	3.033(29)	3.11(3)	3.055	2.9449	3.034		3.0957	2.90(9) [60], 3.0413(21) [64]
$5d_{3/2} \to 6p_{3/2}$	1.336(13)	1.34(2)	1.334	1.2836	1.325		1.3532	1.54(19) [60], 1.349(36) [63], 1.33199(96) [65]
$5d_{3/2} \to 7p_{1/2}$	0.23(3)	0.28(2)	0.261	0.3050			0.2775	
$5d_{3/2} \to 7p_{3/2}$	0.14(2)	0.16(1)	0.147	0.1645			0.1548	
$5d_{3/2} \to 8p_{1/2}$	0.10(5)	0.13(2)	0.119	0.1121			0.1349	
$5d_{3/2} \to 8p_{3/2}$	0.07(3)	0.07(2)	0.070	0.0650			0.0769	
$5d_{3/2} \to 4f_{5/2}$	3.671(35)	3.75(11)						
$5d_{5/2} \to 6p_{3/2}$	4.105(39)	4.02(7)	4.118	3.9876	4.080	4.103	4.1631	4.35(5) [60], 3.945(66) [63], 4.1028(25) [65]
$5d_{5/2} \to 7p_{3/2}$	0.39(6)	0.46(1)	0.432	0.4788		0.451	0.4500	
$5d_{5/2} \to 8p_{3/2}$	0.18(3)	0.21(2)	0.206	0.1926		0.223	0.2239	
$5d_{5/2} \to 4f_{5/2}$	1.002(9)	1.08(4)				0.998		
$5d_{5/2} \to 4f_{7/2}$	4.500(42)	4.84(5)				4.475		
$6p_{1/2} \to 7s_{1/2}$	2.499(23)	2.44(4)	2.493	2.3220			2.4770	
$6p_{1/2} \to 6d_{3/2}$	4.823(45)	4.89(10)					4.8793	
$6p_{3/2} \to 7s_{1/2}$	3.886(37)	3.80(2)	3.882	3.6482			3.8587	
$6p_{3/2} \to 6d_{3/2}$	2.303(22)	2.33(7)					2.3287	
$6p_{3/2} \to 6d_{5/2}$	6.828(64)	6.91(21)					6.9095	

[a]Relativistic coupled-cluster (RCC) method.
[b]Relativistic many-body perturbation theory all-order (RMBPT all-order) method.
[c]Relativistic single-double coupled cluster method with some important valence triple excitations (RCCSDT).
[d]Single-double all-order (SD all-order) method.
[e]Linearized coupled-cluster (LCC) method.
[f]Single-double all-order method including partial triple excitations (SDpT) method.

where the largest difference is no more than 22% occurring at 0.06 a.u. for the $6s_{1/2} \to 8p_{3/2}$ transition.

B. Static dipole polarizabilities

The dynamic dipole scalar and tensor polarizabilities of the state i can be given by

$$\alpha_i^S(\omega) = \sum_n \frac{f_{i\to n}^{(1)}}{\Delta E_{n\to i}^2 - \omega^2} \tag{5}$$

and

$$\alpha_i^T(\omega) = 6\sqrt{\frac{5j_i(2j_i-1)(2j_i+1)}{6(j_i+1)(2j_i+3)}} \times \sum_n (-1)^{j_n+j_i} \begin{Bmatrix} 1 & 1 & 2 \\ j_i & j_i & j_n \end{Bmatrix} \frac{f_{i\to n}^{(1)}}{\Delta E_{n\to i}^2 - \omega^2}, \tag{6}$$

respectively. Here, $\Delta E_{n\to i} = E_n - E_i$ is the transition energy and ω is the laser frequency. j_i is the total angular momenta of the state i. The $E1$ oscillator strength $f_{i\to n}^{(1)}$ is defined as

$$f_{i\to n}^{(1)} = \frac{2|\langle \beta_n j_n \| \boldsymbol{D} \| \beta_i j_i \rangle|^2 \Delta E_{n\to i}}{3(2j_i+1)}. \tag{7}$$

Where β represents all additional angular momenta in addition to the total angular momenta j. The total dynamic dipole polarizability for a specific magnetic component m of the state i can be expressed as

$$\alpha_i(\omega) = \alpha_i^S(\omega) + \frac{3m^2 - j_i(j_i+1)}{j_i(2j_i-1)}\alpha_i^T(\omega). \tag{8}$$

If $\omega = 0$, Eqs. (5), (6), and (8) are reduced to the static polarizabilities.

TABLE IV. Comparison of the static dipole scalar and tensor polarizabilities (a.u.) of the low-lying states $6s_{1/2}$, $6p_{1/2,3/2}$, and $5d_{3/2,5/2}$ of Ba^+ ions with available experimental and theoretical results. (RCICP^C results are calculated by replacing the present RCICP reduced matrix elements of the $6s_{1/2} \rightarrow 6p_{1/2,3/2}$ transitions with the experimental results from Ref. [61]).

Methods	α^S	α^T
	$6s_{1/2}$	
RCICP	121.31(2.79)	
RCICP^C	124.50(10)	
DHFCP-LMM [67]	120.74(9)	
RCCSD(T) [68]	123.7(5)	
RCCSD [69]	123.18	
DK rel. CCSD(T) [70]	123.07	
Nonrel.+sum-over [71]	126.2	
Nonrel.+sum-over [72]	124.7	
SD all-order [59]	124.15	
RCCSD(T) [73]	124.26(1.0)	
SDpT [57]	124.51	
Expt. [74]	123.88(5)	
Expt. [75]	125.5(10)	
Expt. [76]	124.30(16)	
	$6p_{1/2}$	
RCICP	22.22(1.82)	
RCICP^C	21.90(5)	
DHFCP-LMM [67]	22.39(41)	
RCCSD [69]	20.46	
	$6p_{3/2}$	
RCICP	45.77(1.86)	3.26(98)
RCICP^C	45.87(4)	4.09(4)
DHFCP-LMM [67]	45.86(36)	3.110(86)
RCCSD [69]	45.53	4.70
	$5d_{3/2}$	
RCICP	49.81(51)	−21.53(46)
DHFCP-LMM [67]	49.438(26)	−21.403(93)
RCCSD [69]	53.80	−22.92
RCCSD(T) [68]	54.17(250)	−22.19(4)
RCCSD(T) [73]	48.81(46)	−24.62(28)
	$5d_{5/2}$	
RCICP	50.21(56)	−29.43(52)
DHFCP-LMM [67]	49.832(28)	−29.183(120)
LCC [56]	50.6(1.2)	− 29.8(7)
RCCSD [69]	56.53	−31.83
RCCSD(T) [68]	56.87(240)	−32.17(3)
RCCSD(T) [73]	50.67(58)	−30.85(31)

Table IV lists the presently calculated static dipole scalar and tensor polarizabilities for the $6s_{1/2}$, $6p_{1/2}$, $6p_{3/2}$, $5d_{3/2}$, and $5d_{5/2}$ states of Ba^+ ions. These polarizabilities are compared with some available theoretical and experimental results. For the ground state $6s_{1/2}$, the present RCICP result is in excellent agreement with the calculation of the semiempirical-core-potential Dirac-Hartree-Fock approach and the Lagrange-mesh method (DHFCP-LMM) [67], which is similar to our method except that the Lagrange bases are used. The difference is found to be less than 0.5%. However, the present result of 121.31 a.u. is smaller than the experimental [74–76] and other theoretical [57,59,68–73] values. The reason is that the RCICP reduced matrix elements of the $6s_{1/2} \rightarrow 6p_{1/2,3/2}$ transitions are smaller as discussed above. We recalculated the polarizability of the $6s_{1/2}$ state by replacing the RCICP reduced matrix elements of $6s_{1/2} \rightarrow 6p_{1/2,3/2}$ transitions with the experimental values of 3.3251(21) and 4.7017(27) a.u. [61], respectively. Consequently, the resulting polarizability is improved to be 124.50(10) a.u., labeled by RCICP^C in Table IV. This value shows an excellent agreement with the measurements from Refs. [74,76] and the calculations of the SD all-order [59], RCCSDT [73], and SDpT [57] methods. The difference is no more than 0.5%.

TABLE V. Pseudospectral oscillator strength distribution for Ba^{2+} ions. The transition energies $\Delta E_{n\rightarrow i}$ are given in a.u.

n	$\Delta E_{n\rightarrow i}$	f_n
1	1322.014	2.0
2	207.075	2.0
3	194.976	6.0
4	45.200	2.0
5	39.959	6.0
6	30.322	10.0
7	9.476	2.0
8	7.469	6.0
9	3.921	10.0
10	1.433	2.0
11	0.824	6.0

For the $6p_{1/2}$ state, the present RCICP polarizability is also in good agreement with the DHFCP-LMM result [67], while it differs from the RCICP^C result by about 1.5%. For the $6p_{3/2}$ state, the RCICP and RCICP^C scalar polarizabilities are very consistent with each other, and agree excellently with the DHFCP-LMM [67] and RCCSD [69] calculations. However, the present RCICP tensor polarizability is different from the RCICP^C result by about 25%, and the RCICP^C value lies between the DHFCP-LMM and RCCSD values. Moreover, for the $5d_{3/2}$ and $5d_{5/2}$ states, the present RCICP results are in good agreement with the results of the DHFCP-LMM [67], LCC [56], and RCCSD(T) [73].

C. Dynamic polarizabilities

In the calculations of dynamic polarizabilities, the RCICP reduced matrix elements of the $6s_{1/2} \rightarrow 6p_{1/2,3/2}$ transitions are replaced by the experimental values of 3.3251(21) a.u. and 4.7017(27) a.u. [61] to generate the polarizability more accurately. The dynamic polarizability of the core Ba^{2+} is calculated by using a pseudospectral oscillator strength distribution [77–79]. Such a distribution is derived from single-particle Hartree-Fock energies of the core and is listed in Table V.

1. Tune-out wavelengths

Figure 1 shows the dynamic polarizabilities of the $6s_{1/2}$ state, in which three presently obtained tune-out wavelengths are identified with arrows. One of them, 480.658(18) nm, is located in the visible region and lies between the $6s_{1/2} \rightarrow 6p_{1/2}$ and $6s_{1/2} \rightarrow 6p_{3/2}$ transitions. Another two tune-out

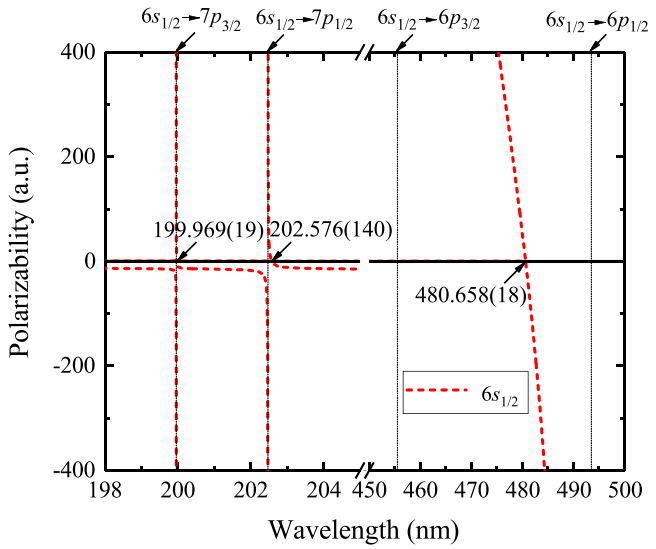

FIG. 1. Dynamic polarizabilities (a.u.) of the ground state of Ba^+ ions. Three tune-out wavelengths are identified with arrows. The vertical dotted lines indicate the positions of the resonant $6s_{1/2} \to np_{1/2,3/2}$ transitions.

wavelengths, 202.576(140) and 199.969(19) nm, are located in the ultraviolet region and are very close to the resonant wavelengths of the $6s_{1/2} \to 7p_{1/2}$ transition and $6s_{1/2} \to 7p_{3/2}$ transition, respectively. Table VI lists the breakdowns of the contributions to the polarizability at these three tune-out wavelengths. The notation "Remains" in the table represents the contributions from highly excited bound and continuum states of the valence electrons. The "Core" denotes the contributions from excitations of core electrons. Apparently, at the tune-out wavelength of about 480 nm, the contributions to the polarizability are dominated by the $6s_{1/2} \to 6p_{1/2}$ and $6s_{1/2} \to 6p_{3/2}$ transitions and the contributions from other transitions are negligibly small. This tune-out wavelength arises from a cancellation of the $6s_{1/2} \to 6p_{1/2}$ and $6s_{1/2} \to 6p_{3/2}$ contributions. Therefore, the relation of the breakdowns of these contributions can be written as

$$0 = f_{6s_{1/2}\to6p_{1/2}}\left[\frac{1}{\left(\Delta E^2_{6p_{1/2}\to6s_{1/2}} - \omega^2\right)} + \frac{\mathcal{R}_{6p}}{\Delta E^2_{6p_{3/2}\to6s_{1/2}} - \omega^2}\right] + \alpha_{\rm rem}(\omega). \quad (9)$$

TABLE VI. Breakdowns of the contributions to the dynamic polarizabilities (a.u.) at different tune-out wavelengths of the ground state of Ba^+ ions.

λ (nm)	∞	480.658(18)	202.576(140)	199.969(19)
$6p_{1/2}$	39.92(5)	−734.59(90)	−8.09(2)	−7.84(1)
$6p_{3/2}$	73.67(8)	723.54(84)	−18.16(15)	−17.59(2)
$7p_{1/2}$	0.01(2)	0.02(2)	14.42(10)	−0.59(74)
$7p_{3/2}$	0.01(1)	0.01(1)	0.08(11)	14.24(71)
Remains	0.28(3)	0.29(3)	0.40(4)	0.41(4)
Core	10.61 [46]	10.73	11.35	11.37
Total	124.50(10)	0.00(1.23)	0.00(22)	0.00(1.03)

Here, $\mathcal{R}_{6p}$ is the ratio of the oscillator strengths of the $6s_{1/2} \to 6p_{1/2,3/2}$ transitions and $\alpha_{\rm rem}(\omega)$ denotes the remainders (excluding the $6s_{1/2} \to 6p_{1/2,3/2}$ transitions) of the polarizability. With the use of Eq. (9) and by combining the accurate experimental oscillator strength of the $6s_{1/2} \to 6p_{1/2}$ transition, the measurements of the 480-nm tune-out wavelength can be used to determine the ratio $\mathcal{R}_{6p}$ with high accuracy. If this tune-out wavelength is measured with infinitely good accuracy, the uncertainty of $\mathcal{R}_{6p}$ arises from the uncertainties of $f_{6s_{1/2}\to6p_{1/2}}$ and $\alpha_{\rm rem}(\omega)$. Combining the most accurate experimental $f_{6s_{1/2}\to6p_{1/2}}$ [61] and the presently calculated $\alpha_{\rm rem}(\omega)$, the uncertainty of $\mathcal{R}_{6p}$ is estimated to be about 0.00009 (i.e., 0.004%). If the uncertainty of measured tune-out wavelength is at a level of 0.001 nm, the uncertainty of $\mathcal{R}_{6p}$ determined by Eq. (9) would be about 0.00013 (approximately 0.005%), which is nearly one order of magnitude smaller than the uncertainty of the most accurate experimental value of 2.1663(32) [61].

2. *Magic wavelengths*

Determining of the magic wavelengths requires calculations of the dynamic polarizabilities of the lower and upper states for given transitions. Figure 2 depicts the dynamic polarizabilities of the $6s_{1/2}$ and $5d_{5/2}$ states with corresponding magic wavelengths identified. The total polarizabilities for each of the magnetic sublevels of the $5d_{5/2}$ state are also shown in which both the scalar and tensor components are included. However, the tensor component can be eliminated by determining the average ac Stark shift [38]. The upper panel of Fig. 2 shows the scalar dynamic polarizabilities of the $6s_{1/2}$ and $5d_{5/2}$ states. The crossings give rise to the average magic wavelengths of the $6s_{1/2} \to 5d_{5/2}$ transition and are identified by arrows. Two visible magic wavelengths are obtained for this transition. One lies between the resonant wavelengths of $6s_{1/2} \to 6p_{3/2}$ and $6s_{1/2} \to 6p_{1/2}$ transitions and the other one is located just exceeding the resonant wavelength of $5d_{5/2} \to 6p_{3/2}$. The lower panel shows the total dynamic polarizabilities of the $6s_{1/2}$ state and the magnetic sublevels $m = 5/2$, $3/2$, and $1/2$ of the $5d_{5/2}$ state. Two magic wavelengths are found for each of the magnetic transitions except for the $6s_{1/2} \to 5d_{5/2}$, $m = 5/2$ transition. There is no magic wavelength near the $5d_{5/2} \to 6p_{3/2}$ resonance for the $6s_{1/2} \to 5d_{5/2}$, $m = 5/2$ transition. This is due to the fact that tensor and scalar contributions of the $5d_{5/2} \to 6p_{3/2}$ transition to total dynamic polarizability of $5d_{5/2}$, $m = 5/2$ state cancel with each other (as shown in Table I of the Supplemental Material [80]). The predicted magic wavelengths are also compared with available experimental [38] and theoretical [56,69] values in Table VII, where a good agreement can be found with the experiment and theoretical results.

It is worth to note that the measurements of these magic wavelengths can be used not only to make an accurate assessment of the room-temperature blackbody radiation (BBR) shift for the Ba^+ clock transition [38], but also to determine the oscillator strength of the $5d_{5/2} \to 4f_{7/2}$ transition. To make a further explanation, Table VIII lists the contributions to the scalar dynamic polarizabilities of the $6s_{1/2}$ and $5d_{5/2}$ states at the magic wavelengths near 653 and 480 nm.

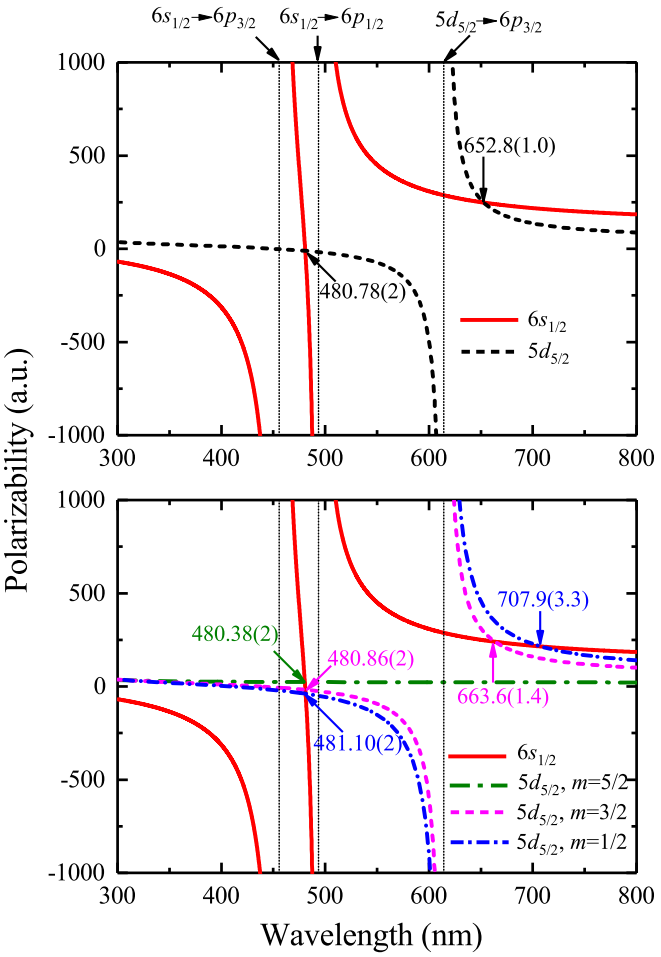

FIG. 2. Dynamic polarizabilities (a.u.) of the $6s_{1/2}$ and $5d_{5/2}$ states of Ba^+ ions. The magic wavelengths are identified by arrows. The vertical dotted lines indicate the positions and wavelengths of the resonant transitions. The upper panel shows the scalar dynamic polarizabilities of the $6s_{1/2}$ and $5d_{5/2}$ states, while the lower panel shows the total dynamic polarizabilities of the $6s_{1/2}$ state and the magnetic sublevels $m = 5/2$, $3/2$, and $1/2$ of the $5d_{5/2}$ state.

As can be seen clearly, the polarizability of the $6s_{1/2}$ state is dominated by the resonant $6s_{1/2} \to 6p_{1/2}$ and $6s_{1/2} \to 6p_{3/2}$ transitions, while the polarizability of the $5d_{5/2}$ state is dominated by the $5d_{5/2} \to 6p_{3/2}$ and $5d_{5/2} \to 4f_{7/2}$ transitions. Based on the definition of the dynamic polarizability

TABLE VIII. Breakdowns of the contributions of individual transitions to the scalar dynamic polarizabilities (a.u.) of the $6s_{1/2}$ and $5d_{5/2}$ states at the magic wavelengths near 653 nm and 480 nm.

	653 nm		480 nm
	RCICP	LCC [56]	RCICP
		$6s_{1/2}$	
$6p_{1/2}$	93.19(13)	93.11(11)	−742.13(28)
$6p_{3/2}$	143.60(18)	143.51(17)	720.21(57)
Remains	0.31(3)	−0.446	0.32(3)
Core	10.68	10.6(5)	10.73
Total	247.78(22)	246.8(6)	−10.87(64)
		$5d_{5/2}$	
$6p_{3/2}$	220.86(1.05)	219.5(5.3)	−39.90(76)
$4f_{7/2}$	13.23(25)	13.08(52)	15.10(28)
Remains	3.01(30)	2.458	3.20(32)
Core	10.68	10.6(5)	10.73
Total	247.78(1.12)	246.8(5.4)	−10.87(87)

in Eq. (5), the relation of the contributions from different transitions can be written as

$$\frac{f_{6s_{1/2}\to6p_{1/2}}}{\Delta E^2_{6s_{1/2}\to6p_{1/2}}-\omega^2}+\frac{f_{6s_{1/2}\to6p_{3/2}}}{\Delta E^2_{6s_{1/2}\to6p_{3/2}}-\omega^2} = \frac{f_{5d_{5/2}\to6p_{3/2}}}{\Delta E^2_{5d_{5/2}\to6p_{3/2}}-\omega^2}+\frac{f_{5d_{5/2}\to4f_{7/2}}}{\Delta E^2_{5d_{5/2}\to4f_{7/2}}-\omega^2} + \left(\alpha^{\rm rem}_{5d_{5/2}}(\omega)-\alpha^{\rm rem}_{6s_{1/2}}(\omega)\right). \quad (10)$$

Here, $\alpha^{\rm rem}_{6s_{1/2}}(\omega)$ and $\alpha^{\rm rem}_{5d_{5/2}}(\omega)$ represent the "Remains" of the $6s_{1/2}$ and $5d_{5/2}$ states given in Table VIII, respectively. By combining the precise measurements of magic wavelengths and oscillator strengths of the $6s_{1/2} \to 6p_{1/2,3/2}$ and $5d_{5/2} \to 6p_{3/2}$ transitions as well as the transition energies from NIST [48], the oscillator strength of the $5d_{5/2} \to 4f_{7/2}$ transition can be determined with the use of Eq. (10). Using the measurements of $f_{6s_{1/2}\to6p_{1/2,3/2}} = 0.3402(5)$, $0.7370(9)$ [61], and $f_{5d_{5/2}\to6p_{3/2}} = 0.1387(2)$ [65], when the uncertainties of measured magic wavelengths are smaller than 0.005 nm, the deduced uncertainties of $f_{5d_{5/2}\to4f_{7/2}}$ should be about 3% which arises from the uncertainties of experimental oscillator strengths and $(\alpha^{\rm rem}_{5d_{5/2}}(\omega)-\alpha^{\rm rem}_{6s_{1/2}}(\omega))$. For example, with the use of the measured magic wavelength 652.913(4) nm [38], the oscillator strength of the $5d_{5/2} \to 4f_{7/2}$ transition is de-

TABLE VII. Magic wavelengths (nm) for the $6s_{1/2} \to 5d_{5/2}$ transition of Ba^+ ions. "Average" represents the magic wavelengths that are determined by the scalar polarizabilities of the $6s_{1/2}$ and $5d_{5/2}$ states. The numbers in parentheses are the uncertainties estimated by the uncertainties of the relevant matrix elements.

$6s_{1/2} \to 5d_{5/2}$							
Average		$m = 5/2$		$m = 3/2$		$m = 1/2$	
RCICP	Refs.	RCICP	RCC [69]	RCICP	RCC [69]	RCICP	RCC [69]
652.8(1.0)	652.913(4) (Expt. [38]) 653.0(1.3) (LCC [56])			663.6(1.4)	666.64	707.9(3.3)	718.18
480.78(2)		480.38(2)	480.26	480.86(2)	480.71	481.10(2)	480.93

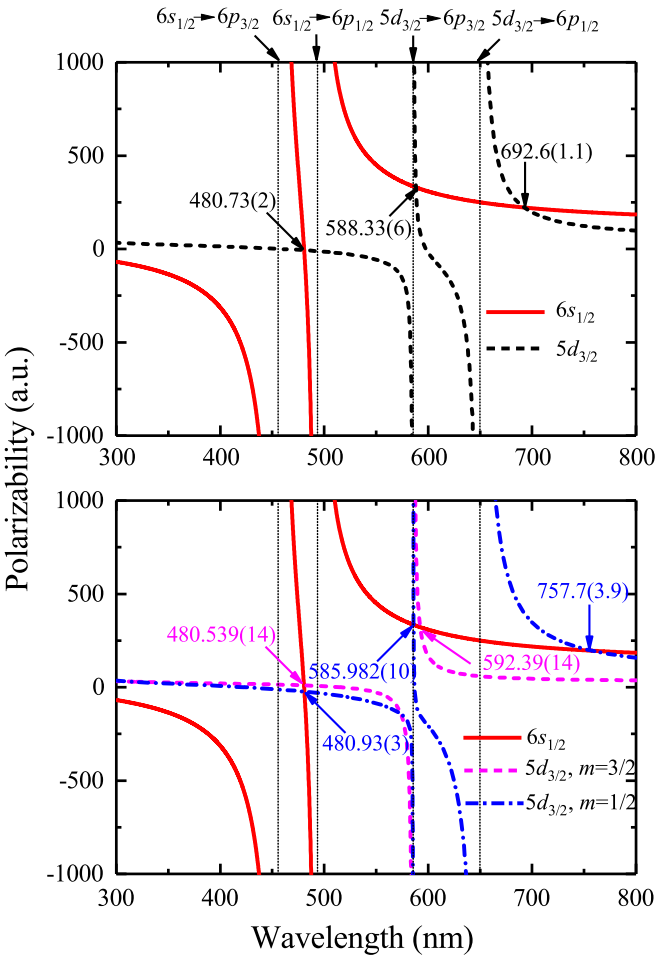

FIG. 3. Same as Fig. 2 but for the $6s_{1/2}$ and $5d_{3/2}$ states of Ba^+ ions.

termined to be 0.466(15), which is in good agreement with theoretical predictions of 0.434 [56] and 0.508(10) [54] as well as the present RCICP result of 0.439(8) that are all derived from the reduced matrix elements and experimental energy levels.

The contributions of individual transitions to the polarizabilities of the $6s_{1/2}$ state and the magnetic sublevels $m = 5/2$, $3/2$, and $1/2$ of the $5d_{5/2}$ state at the corresponding magic wavelengths are given in Table I–III in the Supplemental Materials [80]. These values are useful to experimental determination of the $5d_{5/2} \to 4f_{7/2}$ oscillator strength.

Figure 3 presents the dynamic polarizabilities of the $6s_{1/2}$ and $5d_{3/2}$ states. The upper panel shows the scalar dynamic polarizabilities of the $6s_{1/2}$ and $5d_{3/2}$ states, while the lower panel shows the total polarizabilities of the $6s_{1/2}$ state and the magnetic sublevels $m = 3/2$ and $1/2$ of the $5d_{3/2}$ state.

TABLE IX. Magic wavelengths (nm) for the $6s_{1/2} \to 5d_{3/2}$ transition of Ba^+ ions. The numbers in parentheses are the uncertainties.

$6s_{1/2} \to 5d_{3/2}$				
Average	$m = 3/2$		$m = 1/2$	
RCICP	RCICP	RCC [69]	RCICP	RCC [69]
692.6(1.1)			757.7(3.9)	767.81
588.33(6)	592.39(14)	592.46	585.982(10)	585.98
480.73(2)	480.539(14)	480.44	480.93(3)	480.81

Similarly to the case in Fig. 2, three magic wavelengths are found for the $6s_{1/2} \to 5d_{3/2}$, $m = 1/2$ transition, while only two magic wavelengths are obtained for the $6s_{1/2} \to 5d_{3/2}$, $m = 3/2$ transition since the tensor and scalar contributions of the $5d_{3/2} \to 6p_{1/2}$ transition to the magnetic sublevel $5d_{3/2}$, $m = 3/2$ cancel with each other (as shown in Table V of the Supplemental Material [80]) and the magic wavelength near the $5d_{3/2} \to 6p_{1/2}$ transition vanishes. These magic wavelengths are compared with the RCC results [69] in Table IX. It is found that the present results agree well with the RCC calculations.

Once again, the polarizabilities at the relevant magic wavelengths are also dominated by a few transitions, i.e., the polarizability of the $6s_{1/2}$ state is dominated by the resonant transitions $6s_{1/2} \to 6p_{1/2,3/2}$, while the polarizability of the $5d_{3/2}$ state is dominated by the $5d_{3/2} \to 6p_{1/2,3/2}$ and $5d_{3/2} \to 4f_{5/2}$ transitions. Therefore, by combining the experimental oscillator strengths of $6s_{1/2} \to 6p_{1/2,3/2}$ [61] and $5d_{3/2} \to 6p_{1/2,3/2}$ transitions [65] as well as the transition energies from NIST [48], the measurements of these magic wavelengths can be used to determine the oscillator strength of the $5d_{3/2} \to 4f_{5/2}$ transition. Similarly, if the uncertainties of measured magic wavelengths are smaller than 0.001 nm, the uncertainties of $f_{5d_{3/2}\to4f_{5/2}}$ should be about 3%. Note that the breakdowns of the contributions of individual transitions to the scalar and total dynamic polarizabilities of the $6s_{1/2}$ and $5d_{3/2}$ states at the corresponding magic wavelengths are listed in Tables IV–VI of the Supplemental Material [80].

Figure 4 shows the dynamic polarizabilities of the $6s_{1/2}$ and $6p_{3/2}$ states. Four magic wavelengths are found for each of the transitions, as shown in Table X. It is worth noting that the measurements of the three magic wavelengths near 416 nm can be used to determine the ratio of the oscillator strengths of the $6p_{3/2} \to 6d_{3/2}$ and $6p_{3/2} \to 6d_{5/2}$ transitions. Table XI lists the breakdowns of the contributions to the polarizabilities of the $6s_{1/2}$ and $6p_{3/2}$ states at the magic wavelengths near 416 nm. The contributions to the polarizability of the $6p_{3/2}$ state at these three magic wavelengths are dominated by the $6p_{3/2} \to 6d_{3/2}$ and $6p_{3/2} \to 6d_{5/2}$ transitions. Therefore, the relation of these contributions can be written as

$$\frac{f_{6s_{1/2}\to6p_{1/2}}}{\Delta E^2_{6p_{1/2}\to6s_{1/2}}-\omega^2}+\frac{f_{6s_{1/2}\to6p_{3/2}}}{\Delta E^2_{6s_{1/2}\to6p_{3/2}}-\omega^2}-f_{6p_{3/2}\to6d_{3/2}}\left[\frac{A}{\Delta E^2_{6d_{3/2}\to6p_{3/2}}-\omega^2}+B\frac{\mathcal{R}_{6d}}{\Delta E^2_{6d_{5/2}\to6p_{3/2}}-\omega^2}\right]=\alpha^{\rm rem}_{6p_{3/2}}(\omega)-\alpha^{\rm rem}_{6s_{1/2}}(\omega), \tag{11}$$

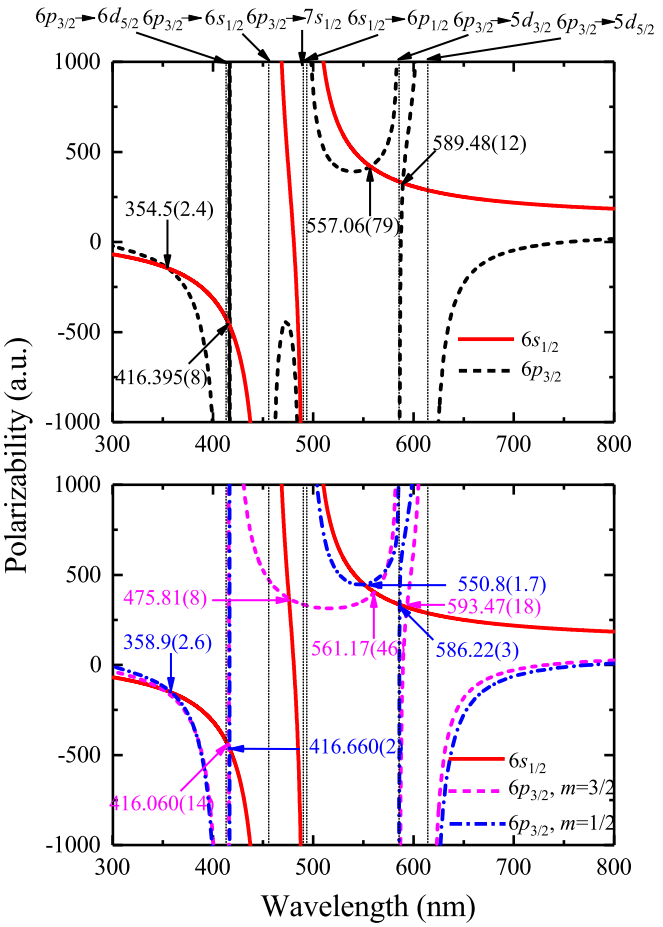

FIG. 4. Same as Fig. 2 but for the $6s_{1/2}$ and $6p_{3/2}$ states of Ba^+ ions.

where $\mathcal{R}_{6d} = f_{6p_{3/2}\to 6d_{5/2}}/f_{6p_{3/2}\to 6d_{3/2}}$. $\alpha^{\rm rem}_{6s_{1/2}}(\omega)$ represents the remaining contributions to the dynamic polarizability of the $6s_{1/2}$ state besides the dominant contributions from the $6s_{1/2} \to 6p_{1/2,3/2}$ transitions, while $\alpha^{\rm rem}_{6p_{3/2}}(\omega)$ has a similar meaning but for the $6p_{3/2}$ state besides the $6p_{3/2} \to 6d_{3/2,5/2}$ transition. Moreover, the coefficients A and B are equal to 1 for the average magic wavelengths, while, for the magic wavelengths corresponding to each of the magnetic transitions, A and B are given by

$$A = 1 + \frac{2\sqrt{6}}{5}\left(\frac{4}{5}m^2 - 1\right) \tag{12}$$

and

$$B = 1 + \frac{\sqrt{6}}{10}\left(1 - \frac{4}{5}m^2\right). \tag{13}$$

Since precise experimental oscillator strengths $f_{6s_{1/2}\to 6p_{1/2}}$ and $f_{6s_{1/2}\to 6p_{3/2}}$ can be obtained, as mentioned above, the measurements of these magic wavelengths near 416 nm could enable an high-precision determination of the ratio between the oscillator strengths of the $6p_{3/2} \to 6d_{3/2}$ and $6p_{3/2} \to 6d_{5/2}$ transitions with the use of Eq. (11).

It is also worth mentioning that the tensor and scalar contributions of the $ns_{1/2} \to 6p_{3/2}$ transitions ($n = 6, 7, 8, \ldots$) to the magnetic sublevel $6p_{3/2}$, $m = 3/2$ cancel with each other (as shown in Tables VIII of the Supplemental Material [80]), and the $ns_{1/2} \to 6p_{3/2}$ ($n = 6, 7, 8, \ldots$) transitions make no contribution to the total polarizability of the sublevel $6p_{3/2}$, $m = 3/2$. As a result, the remainder part of the polarizability of the sublevel $6p_{3/2}$, $m = 3/2$ is much smaller than the remainders of the average polarizability of the $6p_{3/2}$ state and of the polarizability of the sublevel $6p_{3/2}$, $m = 1/2$, as shown in Table XI. The remainder part is found to be less than 1% of the contributions of the $6p_{3/2} \to 6d_{3/2,5/2}$ transitions to the polarizability of the sublevel $6p_{3/2}$, $m = 3/2$. In this case, the value of $\mathcal{R}_{6d}$ determined by the 416.060(14)-nm magic wavelength of the $6s_{1/2} \to 6p_{3/2}$, $m = 3/2$ transition should be more accurate than the values determined by another two 416-nm magic wavelengths, i.e., 416.395(8) nm for the average magic wavelength and 416.660(2) nm for the $6s_{1/2} \to 6p_{3/2}$, $m = 1/2$ transition.

A further analysis for the uncertainties of $\mathcal{R}_{6d}$ is made as follows. If the 416-nm magic wavelength of the $6s_{1/2} \to 6p_{3/2}$, $m = 3/2$ transition is measured with an accuracy of 0.001 nm, the uncertainty of $\mathcal{R}_{6d}$ arises from the uncertainties of the experimental oscillator strengths of the $6s_{1/2} \to 6p_{1/2,3/2}$ transitions, the oscillator strength of the $6p_{3/2} \to 6d_{3/2}$ transition, and $\alpha^{\rm rem}_{6p_{3/2}}(\omega) - \alpha^{\rm rem}_{6s_{1/2}}(\omega)$, and it is estimated to be about 0.2%. Moreover, when the magic wavelength is close to resonant wavelength, radiative line widths of the excited levels would have an impact on polarizabilities. By using the method presented in Refs. [81,82], the dynamic scalar and tensor polarizabilities for the state i should be expressed as

$$\alpha_i^S(\omega) = \sum_n \frac{f^{(1)}_{i\to n}}{2\Delta E_{n\to i}} G_+(n, i, \omega) \tag{14}$$

TABLE X. Magic wavelengths (nm) for the $6s_{1/2} \to 6p_{1/2,3/2}$ transitions of Ba^+ ions. The numbers in parentheses are the uncertainties.

$6s_{1/2} \to 6p_{3/2}$						
Average	$m = 3/2$		$m = 1/2$		$6s_{1/2} \to 6p_{1/2}$	
RCICP	RCICP	RCC [69]	RCICP	RCC [69]	RCICP	RCC [69]
589.48(12)	593.47(18)	593.40	586.22(3)	586.24	599.09(82)	599.28
557.06(79)	561.17(46)	561.01	550.8(1.7)	552.60	468.97(10)	468.90
	475.81 (8)	475.72			451.69(2)	451.73
416.395(8)	416.060(14)	416.06	416.660(2)	416.66		
354.5(2.4)			358.9(2.6)	360.63		

TABLE XI. Breakdowns of the contributions of individual transitions to the polarizabilities (a.u.) of the $6s_{1/2}$ and $6p_{3/2}$ states at the magic wavelengths near 416 nm. $\overline{6p_{3/2}}$ means average polarizability of the $6p_{3/2}$ state, i.e., the tensor components are eliminated by determining the average ac Stark shift.

	416.395(8) nm	416.060(14) nm	416.660(2) nm
	$6s_{1/2}$	$6s_{1/2}$	$6s_{1/2}$
$6p_{1/2}$	−98.60(12)	−98.05(12)	−99.03(13)
$6p_{3/2}$	−374.32(43)	−370.69(41)	−377.24(43)
Remains	0.32(3)	0.32(3)	0.32(3)
Core	10.78	10.78	10.78
Total	−461.82(45)	−457.64(44)	−465.17(45)
	$\overline{6p_{3/2}}$	$6p_{3/2}, m = 3/2$	$6p_{3/2}, m = 1/2$
$6d_{3/2}$	−5215.87(92.06)	−4597.89(56.85)	−5843.34(671.32)
$6d_{5/2}$	4582.84(86.94)	4088.28(100.44)	5085.53(81.29)
Remains	160.44(5.54)	41.20(98)	281.86(7.84)
Core	10.78	10.78	10.78
Total	−461.82(126.74)	−457.64(115.42)	−465.17(676.27)

and

$$\alpha_i^T(\omega) = 6\sqrt{\frac{5j_i(2j_i-1)(2j_i+1)}{6(j_i+1)(2j_i+3)}}\sum_n(-1)^{j_n+j_i} \times \begin{Bmatrix} 1 & 1 & 2 \\ j_i & j_i & j_n \end{Bmatrix} \frac{f^{(1)}_{i\to n}}{2\Delta E_{n\to i}} G_+(n,i,\omega), \quad (15)$$

respectively. The coefficient $G_+(n,i,\omega)$ can be written as

$$G_+(n,i,\omega) = \frac{1}{\Delta E_{n\to i} - \omega - i\Gamma(\omega)/2} + \frac{1}{\Delta E_{n\to i} + \omega + i\Gamma(\omega)/2}. \quad (16)$$

Here, $\Gamma(\omega) = \gamma(\frac{2\Delta E^2_{n\to i}\omega^2}{\Delta E^4_{n\to i}+\omega^4})$ [81]. γ is the full width at half maximum for the case of no external field. The full widths at half maximum of the excited levels $6p_{1/2,3/2}$ were derived from the experimentally measured lifetimes from Refs. [83,84]. Then we recalculated magic wavelengths near 416 nm by using Eqs. (14)-(16) above. Our calculations show that the influence of the radiative line widths on the magic wavelengths near 416 nm is only at the level of 10^{-12} nm. Therefore, the influence of the radiative line widths on the determination of $\mathcal{R}_{6d}$ by the 416-nm magic wavelength is negligible.

The dynamic polarizabilities of the $6s_{1/2}$ and $6p_{1/2}$ states are presented in Fig. 5. Three visible magic wavelengths are found. The transitions from the $6p_{1/2}$ to $ns_{1/2}$ ($n = 6, 7, 8$) and $nd_{3/2}$ ($n = 5, 6, 7$) states make significant contributions to the $6p_{1/2}$ polarizability at these magic wavelengths. Therefore, it is hardly possible to determine the oscillator strengths by measuring these magic wavelengths.

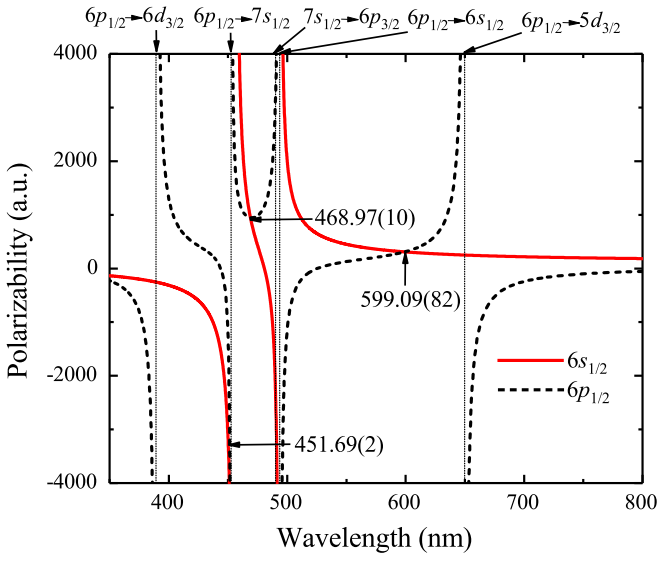

FIG. 5. Dynamic polarizabilities (a.u.) for the $6s_{1/2}$ and $6p_{1/2}$ states of Ba^+ ions. The magic wavelengths are identified by arrows. The vertical dotted lines identify the positions and wavelengths of the resonant transitions.

IV. CONCLUSIONS

The energy levels, $E1$ matrix elements, and the static and dynamic polarizabilities of the low-lying states of Ba^+ ions have been calculated by using the RCICP method. Three tune-out wavelengths of the ground state are determined, among which there is one visible 480-nm tune-out wavelength located between the $6s_{1/2} \to 6p_{1/2,3/2}$ transitions. The 480-nm tune-out wavelength is mainly caused by the cancellation of the contributions from the resonant transitions of $6s_{1/2} \to 6p_{1/2}$ and $6s_{1/2} \to 6p_{3/2}$. Accurate measurements of this tune-out wavelength could be used to determine the ratio of the oscillator strengths of the $6s_{1/2} \to 6p_{1/2}$ and $6s_{1/2} \to 6p_{3/2}$ transitions. If the measurement of tune-out wavelength is at a precision of 0.001 nm, the uncertainty of the predicted oscillator strength ratio of $6s_{1/2} \to 6p_{1/2}$ and $6s_{1/2} \to 6p_{3/2}$ transitions should be at a level of 0.00013 (approximately 0.005%).

In addition, the magic wavelengths of the $6s_{1/2} \to 6p_{1/2,3/2}$ and $6s_{1/2} \to 5d_{3/2,5/2}$ transitions are also determined. The contributions to the dynamic polarizabilities at most of the magic wavelengths are dominated by only a few transitions. We suggest that the measurements of the magic wavelengths for the $6s_{1/2} \to 5d_{5/2}$ transition and its

magnetic sublevel transitions could be used to determine the oscillator strength of the $5d_{5/2} \rightarrow 4f_{7/2}$ transition. Using the existing experimental oscillator strengths, if the uncertainties of measured magic wavelengths are smaller than 0.005 nm, the uncertainties of $f_{5d_{5/2}\rightarrow 4f_{7/2}}$ should be about 3%. For example, the oscillator strength of the $5d_{5/2} \rightarrow 4f_{7/2}$ transition is determined to be 0.466(15) by using the measured magic wavelength of 652.913(4) nm [38]. The measurements of the magic wavelengths for $6s_{1/2} \rightarrow 5d_{3/2}$ transition and its magnetic sublevel transitions could be used to determine the oscillator strength of the $5d_{3/2} \rightarrow 4f_{5/2}$ transition, while the measurements of the magic wavelengths near 416 nm for the $6s_{1/2} \rightarrow 6p_{3/2}$ transition could be used to determine the ratio of oscillator strengths for the $6p_{3/2} \rightarrow 6d_{3/2}$ and $6p_{3/2} \rightarrow 6d_{5/2}$ transitions. If the 416-nm magic wavelength of the $6s_{1/2} \rightarrow 6p_{3/2}$, $m = 3/2$ transition is measured with an accuracy of 0.001 nm, the uncertainty of determined oscillator strength ratio would be about 0.2%.

ACKNOWLEDGMENTS

This work has been supported by the National Key Research and Development Program of China under Grant No. 2017YFA0402300 and the National Natural Science Foundation of China under Grants No. 11774292, No. 11804280, No. 11874051, and No. 11864036. Z.W.W. acknowledges the Major Project of the Research Ability Promotion Program for Young Scholars of Northwest Normal University of China under Grant No. NWNU-LKQN2019-5 and the Youth Science and Technology Talent Promotion Project of Gansu Association for Science and Technology. We would like to thank Dr. Yongjun Cheng for fruitful discussions.

[1] B. J. Bloom, T. L. Nicholson, J. R. Williams, S. L. Campbell, M. Bishof, X. Zhang, W. Zhang, S. L. Bromley, and J. Ye, Nature (London) **506**, 71 (2014).
[2] P. Rosenbusch, S. Ghezali, V. A. Dzuba, V. V. Flambaum, K. Beloy, and A. Derevianko, Phys. Rev. A **79**, 013404 (2009).
[3] B. Arora and B. K. Sahoo, Phys. Rev. A **86**, 033416 (2012).
[4] A. Derevianko and H. Katori, Rev. Mod. Phys. **83**, 331 (2011).
[5] C. W. Chou, D. B. Hume, J. C. J. Koelemeij, D. J. Wineland, and T. Rosenband, Phys. Rev. Lett. **104**, 070802 (2010).
[6] N. Nemitz, T. Ohkubo, M. Takamoto, I. Ushijima, M. Das, N. Ohmae, and H. Katori, Nat. Photonics **10**, 258 (2016).
[7] J. C. Allred, R. N. Lyman, T. W. Kornack, and M. V. Romalis, Phys. Rev. Lett. **89**, 130801 (2002).
[8] G. W. Biedermann, X. Wu, L. Deslauriers, S. Roy, C. Mahadeswaraswamy, and M. A. Kasevich, Phys. Rev. A **91**, 033629 (2015).
[9] I. K. Kominis, T. W. Kornack, J. C. Allred, and M. V. Romalis, Nature (London) **422**, 596 (2003).
[10] R. Dong, R. Wei, Y. Du, F. Zou, J. Lin, and Y. Wang, Appl. Phys. Lett. **106**, 152402 (2015).
[11] R. Charrière, M. Cadoret, N. Zahzam, Y. Bidel, and A. Bresson, Phys. Rev. A **85**, 013639 (2012).
[12] B. Dubetsky and M. A. Kasevich, Phys. Rev. A **74**, 023615 (2006).
[13] M. D. Gregoire, I. Hromada, W. F. Holmgren, R. Trubko, and A. D. Cronin, Phys. Rev. A **92**, 052513 (2015).
[14] J. Ye, D. W. Vernooy, and H. J. Kimble, Phys. Rev. Lett. **83**, 4987 (1999).
[15] H. Katori, T. Ido, and M. Kuwata-Gonokami, J. Phys. Soc. Jpn. **68**, 2479 (1999).
[16] L. Yi, S. Mejri, J. J. McFerran, Y. Le Coq, and S. Bize, Phys. Rev. Lett. **106**, 073005 (2011).
[17] N. Lundblad, M. Schlosser, and J. V. Porto, Phys. Rev. A **81**, 031611(R) (2010).
[18] L. J. LeBlanc and J. H. Thywissen, Phys. Rev. A **75**, 053612 (2007).
[19] J. Catani, G. Barontini, G. Lamporesi, F. Rabatti, G. Thalhammer, F. Minardi, S. Stringari, and M. Inguscio, Phys. Rev. Lett. **103**, 140401 (2009).
[20] R. Chamakhi, H. Ahlers, M. Telmini, C. Schubert, E. M. Rasel, and N. Gaaloul, New J. Phys. **17**, 123002 (2015).
[21] T. Luan, H. Yao, L. Wang, C. Li, S. Yang, X. Chen, and Z. Ma, Opt. Express **23**, 11378 (2015).
[22] M. Hobein, A. Solders, M. Suhonen, Y. Liu, and R. Schuch, Phys. Rev. Lett. **106**, 013002 (2011).
[23] C. D. Herold, V. D. Vaidya, X. Li, S. L. Rolston, J. V. Porto, and M. S. Safronova, Phys. Rev. Lett. **109**, 243003 (2012).
[24] R. H. Leonard, A. J. Fallon, C. A. Sackett, and M. S. Safronova, Phys. Rev. A **92**, 052501 (2015).
[25] F. Schmidt, D. Mayer, M. Hohmann, T. Lausch, F. Kindermann, and A. Widera, Phys. Rev. A **93**, 022507 (2016).
[26] R. Trubko, M. D. Gregoire, W. F. Holmgren, and A. D. Cronin, Phys. Rev. A **95**, 052507 (2017).
[27] W. F. Holmgren, R. Trubko, I. Hromada, and A. D. Cronin, Phys. Rev. Lett. **109**, 243004 (2012).
[28] E. Copenhaver, K. Cassella, R. Berghaus, and H. Müller, Phys. Rev. A **100**, 063603 (2019).
[29] W. Kao, Y. Tang, N. Q. Burdick, and B. L. Lev, Opt. Express **25**, 3411 (2017).
[30] B. M. Henson, R. I. Khakimov, R. G. Dall, K. G. H. Baldwin, L.-Y. Tang, and A. G. Truscott, Phys. Rev. Lett. **115**, 043004 (2015).
[31] Y.-H. Zhang, F.-F. Wu, P.-P. Zhang, L.-Y. Tang, J.-Y. Zhang, K. G. H. Baldwin, and T.-Y. Shi, Phys. Rev. A **99**, 040502(R) (2019).
[32] J. A. Sherman, T. W. Koerber, A. Markhotok, W. Nagourney, and E. N. Fortson, Phys. Rev. Lett. **94**, 243001 (2005).
[33] K. J. Arnold, R. Kaewuam, S. R. Chanu, T. R. Tan, Z. Zhang, and M. D. Barrett, Phys. Rev. Lett. **124**, 193001 (2020).
[34] M. R. Dietrich, N. Kurz, T. Noel, G. Shu, and B. B. Blinov, Phys. Rev. A **81**, 052328 (2010).
[35] I. V. Inlek, C. Crocker, M. Lichtman, K. Sosnova, and C. Monroe, Phys. Rev. Lett. **118**, 250502 (2017).
[36] D. Hucul, J. E. Christensen, E. R. Hudson, and W. C. Campbell, Phys. Rev. Lett. **119**, 100501 (2017).
[37] N. Fortson, Phys. Rev. Lett. **70**, 2383 (1993).
[38] S. R. Chanu, V. P. W. Koh, K. J. Arnold, R. Kaewuam, T. R. Tan, Z. Zhang, M. S. Safronova, and M. D. Barrett, Phys. Rev. A **101**, 042507 (2020).

[39] T. Huber, A. Lambrecht, J. Schmidt, L. Karpa, and T. Schaetz, Nat. Commun. **5**, 5587 (2014).

[40] J. Jiang, J. Mitroy, Y. Cheng, and M. W. J. Bromley, Phys. Rev. A **94**, 062514 (2016).

[41] I. P. Grant, in *Relativistic, Quantum Electrodynamic and Weak Interaction Effects in Atoms*, edited by P. J. Mohr, W. R. Johnson, and J. Sucher, AIP Conf. Proc. No. 189 (AIP, New York, 1989), p. 235.

[42] H. M. Quiney, in *Handbook of Molecular Physics and Quantum Chemistry*, edited by S. Wilson, Vol. 2 (John Wiley and Sons, Ltd., 2003), Chap. 22, p. 423.

[43] I. P. Grant and H. M. Quiney, Adv. At. Mol. Phys. **23**, 37 (1988).

[44] I. P. Grant, *Relativistic Quantum Theory of Atoms and Molecules Theory and Computation* (Springer, New York, 2007).

[45] I. P. Grant, Adv. At. Mol. Opt. Phys. **32**, 169 (1994).

[46] W. Johnson, D. Kolb, and K.-N. Huang, At. Data Nucl. Data Tables **28**, 333 (1983).

[47] I. P. Grant and H. M. Quiney, Phys. Rev. A **62**, 022508 (2000).

[48] A. Kramida, Yu. Ralchenko, J. Reader, and and NIST ASD Team, NIST Atomic Spectra Database (ver. 5.7.1), 2019 (online), available at https://physics.nist.gov/asd.

[49] J. Mitroy, D. C. Griffin, D. W. Norcross, and M. S. Pindzola, Phys. Rev. A **38**, 3339 (1988).

[50] M. Marinescu, H. R. Sadeghpour, and A. Dalgarno, Phys. Rev. A **49**, 5103 (1994).

[51] T. C. Caves and A. Dalgarno, J. Quantum Spectrosc. Radiat. Transfer **12**, 1539 (1972).

[52] S. Hameed, A. Herzenberg, and M. G. James, J. Phys. B **1**, 822 (1968).

[53] P. Hafner and W. H. E. Schwarz, J. Phys. B **11**, 2975 (1978).

[54] B. K. Sahoo, L. W. Wansbeek, K. Jungmann, and R. G. E. Timmermans, Phys. Rev. A **79**, 052512 (2009).

[55] G. Gopakumar, H. Merlitz, R. K. Chaudhuri, B. P. Das, U. S. Mahapatra, and D. Mukherjee, Phys. Rev. A **66**, 032505 (2002).

[56] M. D. Barrett, K. J. Arnold, and M. S. Safronova, Phys. Rev. A **100**, 043418 (2019).

[57] U. I. Safronova, Phys. Rev. A **81**, 052506 (2010).

[58] V. A. Dzuba, V. V. Flambaum, and J. S. M. Ginges, Phys. Rev. A **63**, 062101 (2001).

[59] E. Iskrenova-Tchoukova and M. S. Safronova, Phys. Rev. A **78**, 012508 (2008).

[60] J. Z. Klose, J. R. Fuhr, and W. L. Wiese, J. Phys. Chem. Ref. Data **31**, 217 (2002).

[61] S. L. Woods, M. E. Hanni, S. R. Lundeen, and E. L. Snow, Phys. Rev. A **82**, 012506 (2010).

[62] S. L. Woods, S. R. Lundeen, and E. L. Snow, Phys. Rev. A **80**, 042516 (2009).

[63] N. Kurz, M. R. Dietrich, G. Shu, R. Bowler, J. Salacka, V. Mirgon, and B. B. Blinov, Phys. Rev. A **77**, 060501(R) (2008).

[64] K. J. Arnold, S. R. Chanu, R. Kaewuam, T. R. Tan, L. Yeo, Z. Zhang, M. S. Safronova, and M. D. Barrett, Phys. Rev. A **100**, 032503 (2019).

[65] Z. Zhang, K. J. Arnold, S. R. Chanu, R. Kaewuam, M. S. Safronova, and M. D. Barrett, Phys. Rev. A **101**, 062515 (2020).

[66] J. Jiang, X.-J. Li, X. Wang, C.-Z. Dong, and Z. W. Wu, Phys. Rev. A **102**, 042823 (2020).

[67] L. Filippin, S. Schiffmann, J. Dohet-Eraly, D. Baye, and M. Godefroid, Phys. Rev. A **97**, 012506 (2018).

[68] J. Kaur, S. Singh, B. Arora, and B. K. Sahoo, Phys. Rev. A **95**, 042501 (2017).

[69] J. Kaur, S. Singh, B. Arora, and B. K. Sahoo, Phys. Rev. A **92**, 031402(R) (2015).

[70] I. S. Lim and P. Schwerdtfeger, Phys. Rev. A **70**, 062501 (2004).

[71] I. Miadoková, V. Kellö, and A. J. Sadlej, Theor. Chem. Acc. **96**, 166 (1997).

[72] S. H. Patil and K. T. Tang, J. Chem. Phys. **106**, 2298 (1997).

[73] B. K. Sahoo, R. G. E. Timmermans, B. P. Das, and D. Mukherjee, Phys. Rev. A **80**, 062506 (2009).

[74] E. L. Snow and S. R. Lundeen, Phys. Rev. A **76**, 052505 (2007).

[75] T. F. Gallagher, R. Kachru, and N. H. Tran, Phys. Rev. A **26**, 2611 (1982).

[76] E. L. Snow, M. A. Gearba, R. A. Komara, S. R. Lundeen, and W. G. Sturrus, Phys. Rev. A **71**, 022510 (2005).

[77] A. Kumar and W. J. Meath, Mol. Phys. **54**, 823 (1985).

[78] J. Mitroy and M. W. J. Bromley, Phys. Rev. A **68**, 052714 (2003).

[79] D. J. Margoliash and W. J. Meath, J. Chem. Phys. **69**, 2267 (1978).

[80] See Supplemental Material at http://link.aps.org/supplemental/10.1103/PhysRevA.103.032803 for additional tables of the contributions of individual transitions to the dynamic polarizabilities at the magic wavelengths.

[81] C. M. J. Wijers, Phys. Rev. A **70**, 063807 (2004).

[82] K. D. Bonin and V. V. Kresin, *Electric-Dipole Polarizabilities of Atoms, Molecules, and Clusters* (World Scientific, Singapore, 1997).

[83] P. Kuske, N. Kirchner, W. Wittmann, H. J. Andrä, and D. Kaiser, Phys. Lett. A **64**, 377 (1978).

[84] H. J. Andrä, in *Beam-Foil Spectroscopy, Collisional and Radiative Processes*, edited by I. A. Sellin and D. J. Pegg (Plenum, New York, 1976), Vol. 2, p. 835.